

# Accelerated Screening of Protein–Ligand Interactions via Parallel $T_2$ -Weighted $^{19}\text{F}$ -MRI

Dilara Faderl, Ajmal Chenakkara, Mazin Jouda, Neil MacKinnon,\* Alvar D. Gossert, and Jan G. Korvink\*

Cite This: <https://doi.org/10.1021/acs.analchem.4c00333>

Read Online

ACCESS |



Metrics &amp; More



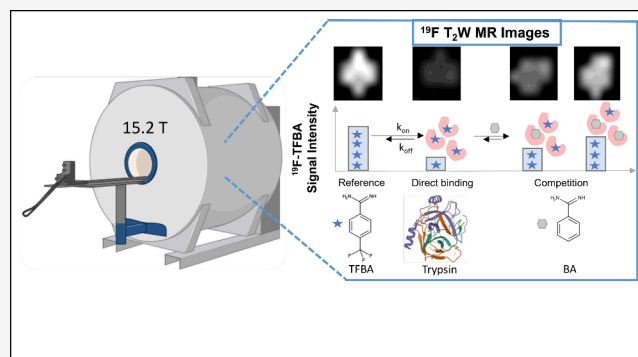
Article Recommendations



Supporting Information

**ABSTRACT:** In drug discovery, ligands are sought that modulate the (mal-)function of medicinally relevant target proteins. In order to develop new drugs, typically a multitude of potential ligands are initially screened for binding and subsequently characterized for their affinity. Nuclear magnetic resonance (NMR) is a well-established and highly sensitive technology for characterizing such interactions. However, it has limited throughput, because only one sample can be measured at a time. In contrast, magnetic resonance imaging (MRI) is inherently parallel and MR parameters can conveniently be encoded in its images, potentially offering increased sample throughput. We explore this application using a custom-built 9-fold sample holder and a  $^{19}\text{F}$ -MRI coil. With this setup, we show that ligand binding can be detected by  $T_2$ -weighted  $^{19}\text{F}$ -MRI using 4-(trifluoromethyl)benzamide (TFBA) and trypsin as the reporter ligand and target protein, respectively.

Furthermore, we demonstrate that the affinity of nonfluorinated ligands can be determined in a competition format by monitoring the dose-dependent displacement of TFBA. By comparing  $^{19}\text{F}$ - $T_2$ -weighted MR images of TFBA in the presence of different benzamide (BA) concentrations—all recorded in parallel—the affinity of BA could be derived. Therefore, this approach promises parallel characterization of protein–ligand interactions and increased throughput of biochemical assays, with potential for increased sensitivity when combined with hyperpolarization techniques.



## INTRODUCTION

Drugs can modulate the function of target proteins in many different ways, but any drug action is based on a molecular interaction. Thus, identifying such interactions is typically the start of every drug discovery campaign. This requires screening of the largest possible chemical space (e.g., compound libraries), which quickly makes the experiment intractable, given the sheer number of measurements required. Therefore, high-throughput screening (HTS) methods have been used to accelerate drug discovery.<sup>1–3</sup> In subsequent steps, initially identified binders are characterized more deeply in terms of their affinity, their binding mode, etc. This is achieved by screening different parameters for each compound, for instance, concentration-dependent activity. Therefore, screening and subsequent characterization require a large number of experiments, which ideally should be parallelized. Could the dense parallelization offered in magnetic resonance (MR) images be leveraged for such studies?

Magnetic resonance imaging (MRI) takes advantage of nuclear magnetic resonance (NMR) and spatial resolution at the same time. NMR is a well-established and highly sensitive technique for detecting ligand binding. Several NMR parameters are modulated in a system consisting of a small (drug) molecule and a large (protein) molecule that interact.<sup>4</sup> The most popular property to exploit is the molecular motion of the small

molecule, since it can easily change 100-fold upon binding to a biomacromolecule. The ligand tumbling rate difference between free and bound states correlates with a change in  $T_2$  relaxation, which can be conveniently encoded in  $T_2$ -weighted MR images. A significant advantage of MRI over alternative imaging methods is the ability to encode various types of contrast into the image, reflecting spin density, relaxation properties of the nuclei ( $T_1$ ,  $T_2$ ), and their transport (diffusion, flow).

However, what standard MRI experiments do not offer is the chemical shift resolution allowing differentiation of different molecules in an experimental solution, that is, the solvent, buffer components, ligands, and proteins. A notable exception is chemical shift imaging (CSI), which allows one to obtain resolved NMR spectra of voxels.<sup>5</sup> With a sufficient signal-to-noise ratio (SNR), this technique reveals detailed information; however, in order to use MRI in a high throughput sample screening context, a simplified spectrum is required, which can

**Received:** January 17, 2024

**Revised:** April 22, 2024

**Accepted:** April 29, 2024

be achieved by recording  $^{19}\text{F}$  spectra. Here, several advantages come together:

- (i)  $^{19}\text{F}$  has essentially 100% natural abundance;
- (ii) fluorinated druglike ligands typically contain only one F atom or one  $\text{CF}_3$  group of equivalent F atoms, leading to a single resonance in the NMR spectrum;
- (iii)  $^{19}\text{F}$  spectra are typically background-free, such that no special considerations apply when choosing a physiological buffer;
- (iv)  $T_2$  relaxation is particularly sensitive to the environment for  $^{19}\text{F}$  nuclei, due to large chemical shift anisotropy and exchange broadening typically observed for ligands exchanging between free and bound states;<sup>6,7</sup> and
- (v) measurement time can be reduced by avoiding full FID measurement and localized shimming routines and, instead, taking advantage of  $T_2$  contrast to report on ligand binding.

Taken together, the single, intense fluorine signal paired with exceptionally strong binding contrast makes  $^{19}\text{F}$   $T_2$ -weighted MRI an ideal candidate for the detection of ligand binding.

Acquisition of MRI spectra is relatively slow, but parallelization can conveniently be achieved by measuring several samples at once, exploiting the spatial resolution of MR images. The contrast in a magnetic resonance image is delivered at the spatial resolution of a pixel. For an  $n$ -dimensional image, at a one-dimensional resolution of  $d$ , this implies  $d^n$  separate experiments in the image, which, if successful, represents a remarkably dense parallelization of the experiment. For example, it is routine practice to obtain images at 256 pixels per axis, implying  $256^3 = 16\,777\,216$  separate NMR experiments in the MR image. Thus, the challenging question becomes how to arrange the experiment so that each dimension of the image efficiently contributes to the overall experiment.

There are several methodologies that can greatly contribute to the faster acquisition of MR images. One of them is a chemical shift imaging method that allows the parallel detection of multiple spectra including different Larmor frequencies from the bundle of capillaries resolved in an image.<sup>5</sup> Another example, time-optimal schemes exist for traversing  $k$ -space, such as sparse sampling, relying on the fact that the density of information in  $k$ -space is not isotropically distributed. On the other hand, parallel imaging methods such as PATLOC<sup>8,9</sup> use a curvilinear coordinate system for  $k$ -space, combined with a semidiscrete partition of the imaging space, to achieve local orthogonality and, hence, rapid acquisition of the  $k$ -space data. If applied successfully, the dense parallelization reflected in an MR image could be used to efficiently screen large parameter or chemical spaces and, as an example, significantly contribute to accelerating image-based drug screening.

In this work, we demonstrate an approach to image-based drug screening using  $^{19}\text{F}$   $T_2$ -weighted MRI. As a model ligand–protein system, the ligand 4-(trifluoromethyl)benzamidinium (TFBA, reporter) was used, together with a nonfluorinated ligand benzamidinium (BA, competitor) and the protein serine protease trypsin from *B. taurus*. Using  $^{19}\text{F}$   $T_2$ -weighted MRI, we could detect the binding between TFBA and trypsin directly by observing the  $^{19}\text{F}$ -signal of TFBA. Subsequently, binding of the nonfluorinated competitive ligand BA could be detected by displacement of the TFBA reporter. In a dose-dependent competition experiment with the competitor ligand BA at different concentrations in the presence of TFBA and trypsin, the affinity of BA could be determined in a quantitative manner

in a single parallelized experiment. By taking advantage of pixel-based parallelization, a factor of 9 in sample parallelization, yielding a factor of 3 in measurement acceleration, is demonstrated, suggesting that complete binding curves (dose-dependent screening) could be measured in a single measurement.

## EXPERIMENTAL METHODS

**$^{19}\text{F}$  Hardware.** The measurements were conducted using a custom-designed RF coil operating at a frequency of 612 MHz, which corresponds to the Larmor frequency of  $^{19}\text{F}$  in a 15.2 T homogeneous magnetic field. This coil was engineered based on an Alderman–Grant topology, due to its inherently low inductance and low electric field. As a result, it features a sufficiently high self-resonance frequency, providing a broad tunability range, making it particularly well-suited for isotopes with high gyromagnetic ratios, such as  $^1\text{H}$  and  $^{19}\text{F}$ .

Following the geometric optimization strategy outlined by Mispelter et al.,<sup>10</sup> we fashioned a coil with specific dimensions: a diameter ( $d$ ) of 15 mm and a length ( $l$ ) of 21 mm, resulting in an  $l/d$  ratio of 1.4. This ratio was chosen to achieve optimized sensitivity, denoted as  $B_1/(ir^{1/2})$ , where  $B_1$  represents the field intensity, and  $r$  is the resistance of the coil. The coil itself is constructed from a 35- $\mu\text{m}$ -thick adhesive copper foil, meticulously wound around a three-dimensional (3D) filament-based printed support, produced using a PLA printer (Ultimaker 2+). The constructed coil is shown in Figure 1a.

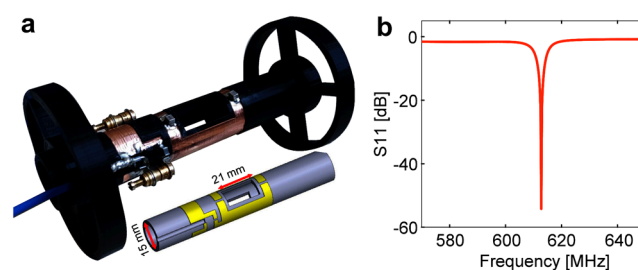


**Figure 1.** (a) Alderman–Grant coil designed to operate at 612 MHz corresponding to the  $^{19}\text{F}$  NMR Larmor frequency at 15.2 T. A 3D-printed coil holder (black) and coaxial RF cable (blue) are also shown. The schematic insert above shows the geometry of the coil tracks. (b)  $S_{11}$  reflection curve of the unloaded Alderman–Grant resonator.

To facilitate tuning and matching, the coil was capacitively coupled to a coaxial cable through two high-Q nonmagnetic trimmer capacitors (Model V9000, Voltronics). Figure 1b illustrates the  $S_{11}$  reflection curve of the unloaded coil, tuned and matched at 612 MHz. In this configuration, the unloaded Q-factor registered at 151, which was reduced to 136 when loaded with a 10-mm glass tube that was filled with distilled water.

**Sample Holder.** To accommodate the glass capillary samples used in this study, a modular PLA 3D printed (Ultimaker 2+) sample holder was developed which fixed the nine sample tubes in position, as shown in Figure 2. The entire sample assembly was inserted into the RF coil horizontally.

**Sample Preparation.** Trypsin from bovine pancreas (Sigma-Aldrich, Catalog No. T9935), 4-(trifluoromethyl)-benzamidinium (TFBA) (Enamine, Catalog No. EN300-73109), and benzamidinium (BA) (Sigma-Aldrich, Catalog No. 434760) were used as a target protein, reporter, and competitor ligand, respectively. All solutions were prepared in phosphate-buffered



**Figure 2.** Sample holder assembly, 3D-printed using PLA. Nine individual sample capillaries, each with an OD of 2.4 mm, and filled with a sample volume of 150–200  $\mu\text{L}$ , were thus accommodated.

saline solution (PBS, 1 $\times$ , pH 7.4, ThermoFisher, Catalog No. 10010-015).

Ligand-observed  $^{19}\text{F}$ -MRI experiments were carried out with different concentrations of trypsin, TFBA, and BA. First, the samples were prepared in a PBS buffer as a stock solution to ensure the same relative concentrations in all experiments. Then they were diluted to their final concentrations and placed into a 2.4-mm-OD glass capillary (CM Scientific) with a microliter syringe (Hamilton Central Europe S.R.L.). The glass capillaries were sealed by UV glue (Delo Photoband). All samples were prepared fresh on the day of measurement and stored in a cool transport box. Afterward, nine samples were inserted into a home-built sample holder (detailed in the “Sample Holder” section prior to acquisition).

**MRI  $T_2$ -Relaxation Experiments.** All  $^{19}\text{F}$ - $T_2$  relaxation experiments were performed using a Bruker 650 MHz (15.2 T) BioSpec imaging system (Bruker BioSpin, Ettlingen) with a 15-mm-diameter home-built  $^{19}\text{F}$  coil. MR images were acquired by using dedicated protocols using spin and gradient-echo pulse sequences. A typical MSME (multislice, multiecho) experiment used a field of view (FOV) of 20 mm  $\times$  20 mm and a slice thickness (SL) of 10 mm, a matrix size of (MTX) of 32  $\times$  32, repetition time (TR) of 7218 ms, and 20 averages, unless otherwise indicated. This MSME protocol enabled one to measure  $T_2$ -mapping with a sufficient number of echo time (TE) parameters necessary to observe the large range of TFBA  $T_2$ -relaxation times, depending on the binding conditions (see Table S1 in the Supporting Information). We have optimized the imaging parameters (FOV, MTX, and SL) and acquired the same experiment with two different spin–echo experiments (see Figures S2 and S3 in the Supporting Information).

**Data Analysis.** A region of interest (ROI) was drawn over  $T_2$ -weighted images, and their ROIs were analyzed to determine relaxation times using the image analysis function of ParaVision 360 (version 360.3). The ROI calculations were made on magnitude-reconstructed images. The SNR values were determined by the single image method, according to the National Electrical Manufacturers Association (NEMA) standards,<sup>11</sup> i.e., the mean signal intensities in the area of interest (signal ROI) and the background (noise ROI) were quantified and the SNR calculated by dividing the signal ROI by the noise ROI (see Figure S1 in the Supporting Information).

The representative findings were confirmed in at least three independent experiments. Statistical analysis was performed using OriginPro 2023 (Originlab Corporation, Wellesley Hills, MA, USA).

## RESULTS

**Probe Characterization–SNR.** To best exploit MRI parallelization, it was first necessary to identify the concentration regime that yielded sufficient SNR for the reporter molecule TFBA using the custom  $^{19}\text{F}$  probe. A FLASH sequence was used on a collection of five capillary samples, carrying TFBA in concentrations ranging from 3–50 mM. Using the imaging parameters given in Figure 3, resulting in voxel volumes of  $\sim 4.4$



**Figure 3.**  $^{19}\text{F}$  limit of detection of TFBA in a capillary system. Five different TFBA concentrations (white) and their calculated SNR (yellow) values are shown from the FLASH experiment in one acquisition experiment. The imaging parameters were as follows: FOV, 30 mm  $\times$  30 mm; MTX, 32  $\times$  32; SL, 5 mm; TR/TE = 100/4 ms; NEX, 200; TA, 10 min, 40 s. SNR was calculated as described in the Experimental Methods section, taking a slice ROI area covering 3.55 voxels, with a volume of 4.4 mm<sup>3</sup> per sample.

$\mu\text{L}$ , it was found that 3 mM TFBA was not sufficient to observe a signal (details on arriving at these imaging parameters can be found in the Supporting Information). Conversely, 50 mM was more than sufficient; however, significantly more protein would be needed at this concentration for the binding assay. A TFBA concentration of 25 mM represented a good compromise between sufficient SNR (17) such that the quantification threshold was achieved (SNR > 10) and reduced the required amount of protein for the binding assays.

**Proof of Concept.** We performed initial experiments to establish that ligand binding can be detected by encoding  $T_2$  contrast into an MR image and that reporter displacement experiments are possible. To this end, a quantitative spin–echo imaging protocol, multislice multiecho (MSME), was used to extract  $T_2$  values of free TFBA, TFBA in the presence of trypsin (direct detection of binding), and third, TFBA in the presence of both trypsin and BA (indirect detection of binding) (Figure 4). As expected, the  $^{19}\text{F}$   $T_2$  of free TFBA ( $T_{2,f} = 950$  ms) was reduced by 75% in the presence of trypsin (167:1 TFBA:trypsin,  $T_{2,nc} = 230$  ms, where nc denotes noncompetition). The fit was to a single exponential, suggesting that TFBA is in fast exchange, which was confirmed by spectroscopic measurements in which a single  $^{19}\text{F}$  resonance was observed in the presence of trypsin.<sup>12</sup> In a next step, by adding BA as a competitor (2.5:1, TFBA:BA), the TFBA reporter  $^{19}\text{F}$   $T_{2,c}$  recovered to 70% of the  $T_{2,f}$  value ( $T_{2,c} = 740$  ms, where c denotes competition), demonstrating a shift in binding equilibrium with BA now favored as the stronger binding ligand for trypsin, compared to TFBA. Thus, we could demonstrate that (i) direct detection of the binding of a fluorinated ligand is possible with our custom MRI setup and (ii) binding of a nonfluorinated molecule can also be detected in a competition format.

The concept of parallelized MRI-based drug screening is presented in Figure 5. For demonstration, two titration series were measured in a single imaging experiment: first, a series of samples with a fixed quantity of TFBA and varying

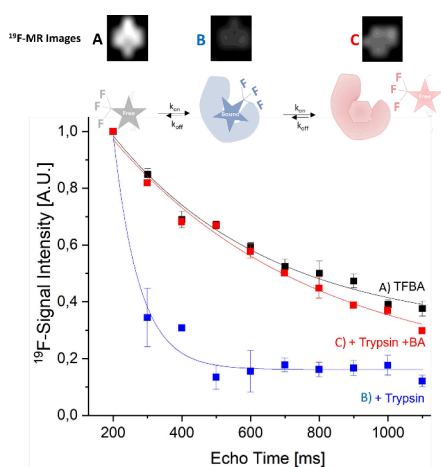


**Figure 4.** Transverse relaxation time dependence on binding between trypsin and its reporter and competitor ligands, TFBA and BA. Spin-echo intensities extracted from the chosen ROI of the MR-image averaged 20 scans, of 25 mM TFBA obtained in the absence (black) and presence of 150  $\mu$ M trypsin (blue), and in the presence of both 150  $\mu$ M trypsin and 10 mM benzamidine (red).  $T_2$  relaxation times were obtained by fitting the mean of three replicate measurements to a single exponential (error bars are  $\pm$  standard deviation);  $T_{2,f} = 952$  ms,  $T_{2,nc} = 231$  ms, and  $T_{2,c} = 738$  ms, (ParaVision) with a fit quality ( $R^2$ ) of 0.98, 0.98, and 0.97 (originLab), respectively. The corresponding relaxation rates are  $R_{2,f} = 1.05$  s $^{-1}$ ,  $R_{2,nc} = 4.33$  s $^{-1}$ , and  $R_{2,c} = 1.36$  s $^{-1}$ .

concentrations of trypsin, and second, a series of samples with a fixed concentration of trypsin and TFBA and varying concentrations of the competitor BA. In this experiment, nine samples could be measured in parallel, translating to a factor of 3 in measurement acceleration.

**Direct Binding Detection.** Binding of TFBA to trypsin can easily be detected on the plain MR image. In Figure 5, the sample of free TFBA was placed in the center of the sample holder (Figure 5A). In position B, 25  $\mu$ M of trypsin was added to the 25 mM TFBA solution (corresponding to a trypsin:TFBA ratio of 1:1000). The decrease in intensity is clearly apparent on this single  $T_2$ -weighted image, thus enabling a quick screening of binders. The  $T_2$  contrast becomes larger at increasing trypsin concentrations. Samples B–E were a titration series of increasing trypsin concentration, from 25  $\mu$ M to 150  $\mu$ M. With increasing trypsin concentration, the  $^{19}$ F signal intensity was observed to decrease, with up to 60% signal attenuation at the highest concentration (Figure 6). Using sample A to normalize the intensities of all other samples in the experiment,  $R_2$  rates (defined as  $R^2 = 1/T_2$ ) could be extracted for all of these samples (Figure 6).

**Competition Screening.** The strong difference in  $R_2$  of TFBA in its free state and in the presence of trypsin opens the possibility to set up a reporter assay. At concentrations of 25 mM TFBA and 150  $\mu$ M trypsin, the high sensitivity of the TFBA signal and the strong contrast from binding effects open a suitable assay window. In this way, nonfluorinated ligands, here BA, could be tested for binding. Indeed, the  $^{19}$ F-signal intensity of TFBA was recovered when adding the nonfluorinated competitor BA to the solution, as demonstrated in samples F–I (Figure 5), where BA was titrated with concentrations ranging from 1 mM to 50 mM. The signal intensities and  $^{19}$ F relaxation rates are plotted in Figure 7. Even at 1 mM BA, nearly 90% of the  $^{19}$ F signal intensity from TFBA could be recovered, showing that competitors can be screened at much lower concentrations,

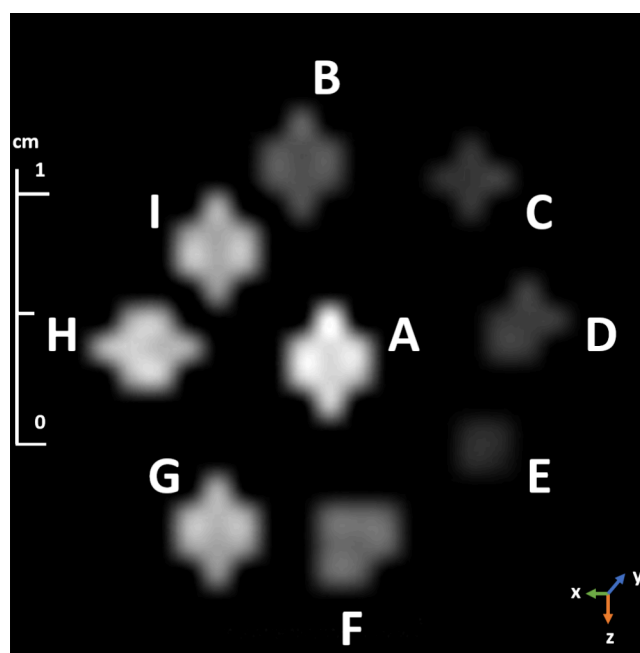


**Figure 5.**  $^{19}$ F  $T_2$  map of TFBA obtained using MSME. Samples for noncompetitive binding to trypsin and competitive binding in the presence of BA were measured in a single experiment. The MSME experiment was a collection of nine samples with 10 echo times, ranging from 200 ms to 1100 ms. Fixed amounts of TFBA (A, 25 mM) were added to trypsin in different concentrations (B, 25  $\mu$ M; C, 50  $\mu$ M; D, 75  $\mu$ M; and E, 150  $\mu$ M) for noncompetitive experiments. Different concentrations of BA (F, 1 mM; G, 10 mM; H, 25 mM; and I, 50 mM) was then added to the fixed TFBA and trypsin at 150  $\mu$ M for the competition format. The imaging parameters were as follows: FOV, 20 mm  $\times$  20 mm; MTX, 32  $\times$  32; SL, 10 mm; TR/TE = 5418/100 ms; NEX, 20. The full set of 10 echo experiments required 76 min. The image displayed was obtained at an echo time of 200 ms. The crosslike shapes are due to a partial volume effect resulting from pixel dimensions approaching the diameter of the sample capillary.

which would make less-soluble compounds accessible to this assay.

**Affinity Determination.** The dose-dependent behavior observed in the competition experiment and the quantitative nature of the relaxation data obtained enable calculation of the dissociation constant of the competitor BA (termed  $K_I$  to distinguish it from the  $K_D$  of the reporter TFBA). The dissociation constant of the competitor BA ( $K_I$ ) was determined from the fraction of displaced reporter ligand TFBA in the presence of trypsin and under competition with the trypsin inhibitor BA (F; see eq 1).  $F$ -values (expressed as a percentage) were calculated based on the reporter relaxation rates in the free state ( $R_{2,f}$ ), and in the absence of a competitor ligand ( $R_{2,nc}$ ) and in the presence of a competitor ligand BA ( $R_{2,c}$ ), together with trypsin:<sup>7</sup>

$$F (\%) = 100 \times \left( 1 - \frac{R_{2,c} - R_{2,f}}{R_{2,nc} - R_{2,f}} \right) \quad (1)$$

With knowledge of the known TFBA dissociation constant ( $K_D = 142$   $\mu$ M),<sup>12</sup> eq 2 was used to derive  $K_I$  for competitor ligand BA:<sup>7</sup>

$$K_I = \frac{(100 - F)[C]K_D}{F([L_T] + K_D)} \quad (2)$$

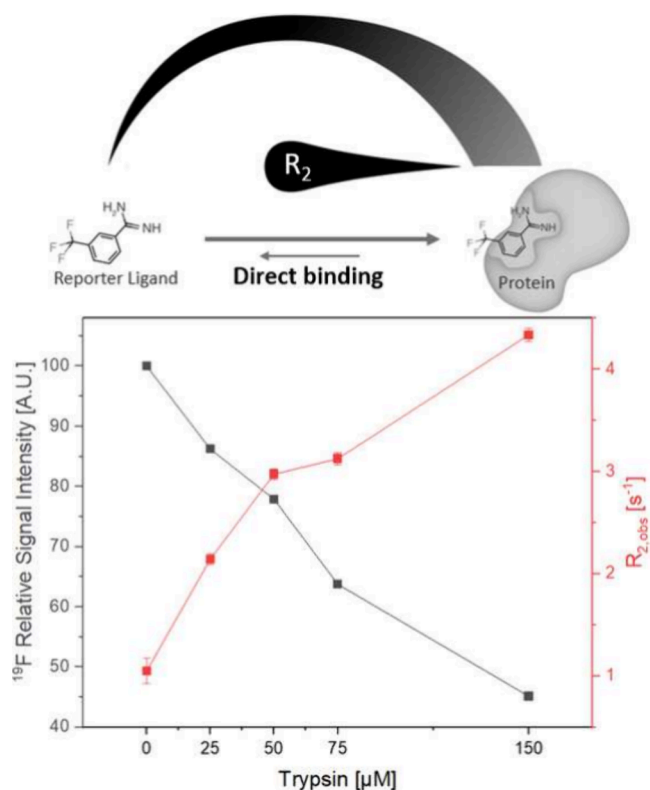


**Figure 6.** Dependence of the TFBA <sup>19</sup>F signal intensity (black) and  $R_2$  rates (red) on titrating trypsin ([TFBA] = 25 mM). <sup>19</sup>F-signal intensities are normalized with the sample without trypsin.

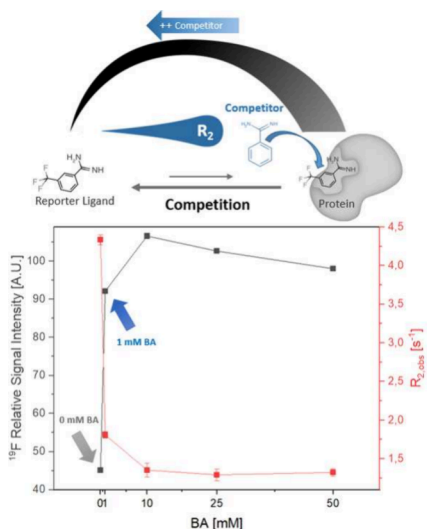


**Figure 7.** TFBA <sup>19</sup>F signal intensity (black) and  $R_2$  rates (red) in the competitive assay. BA was titrated with [TFBA] = 25 mM and [trypsin] = 150 μM. Lines connecting the data points are intended to guide the eye.

The dissociation constant of the competing ligand yields  $K_1 = 5.8$  μM at a total reporter ligand concentration ( $L_T$ ) of 25 mM, and a concentration of free competing ligand ( $C$ ) of 10 mM. The  $R_2$  values obtained from the experiments are given in Figures 6 and 7.

## DISCUSSION

Rapid imaging techniques aiming to detect ligand binding have been demonstrated using various forms of MRI contrast. Examples include using <sup>1</sup>H-MRI to monitor relaxation changes of the surrounding water with a fast spin echo (FSE) sequence,<sup>13</sup> and using paramagnetic MRI contrast agents to shorten the  $T_1$  relaxation and build a chelate complex around ligands.<sup>14</sup> Aside from access to these contrast mechanisms, an additional advantage of MRI is the ability to spatially localize signals originating from multiple samples within a single measurement. Through this form of parallelization, we could simultaneously detect <sup>19</sup>F-signals of a reporter ligand (TFBA) in nine different binding experiments, determine  $T_2$ -relaxation time modulation upon direct and competitive binding (i.e., presence of the target ligand BA).

Using <sup>19</sup>F MRI in a competitive ligand binding assay has several advantages. Since the reporter ligand is the only source of <sup>19</sup>F, there is a direct measurement of its population distribution between bound and free states without background interference. As the reporter has a relatively weak binding interaction (compared to a typical drug), the concentration can be increased so that there is sufficient SNR to obtain MR images in a reasonable measurement time. The sensitivity to competitor binding becomes relatively high, since observation of the competing ligand binding depends on the signal detection limit of a reporter ligand.<sup>15</sup> Thus, only a small amount of the competitor ligand (drug candidate of interest) and protein are required. In our experiment, pixel volumes were ~4 μL, corresponding to 300 nmol of <sup>19</sup>F nuclei using 25 mM TFBA. The sensitivity could be improved by using smaller RF coils (thereby increasing the filling factor); however, a tradeoff is required in the case of sample parallelization, because the coil volume must accommodate multiple samples. Another option would be to combine parallel detection with hyperpolarization of the reporter ligand, which would allow much smaller individual samples. Even without these possible future modifications, in the present competitive assay 1 mM of the competitive ligand was sufficient to recover 90% of the TFBA signal and, thus, the MRI-based version of the assay is sensitive to (at least) 4 nmol of ligand. Note that, in a screening context, only one concentration of the competing molecule is needed to characterize the binding affinity.<sup>16</sup>

To accelerate drug discovery, it is important that the method can be applied by the general NMR-based drug screening community. The design presented (RF coil and capillary bundle) is such that the size of the system can be adapted to fit in a standard vertical-bore NMR magnet, particularly when considering the advances in micromanufacturing. For instance, high-resolution 3D printing can be employed to realize scaffolds with large numbers of microcapillaries. Future improvements can leverage microfabrication technologies on flexible substrates to realize miniaturized coils that improve the filling factor. Note that our implementation uses imaging principles, so a three-axis gradient system is needed, which may be less available, although clever use of a single-axis gradient and/or the room-temperature shims could be imagined to achieve similar parallelization. Generally, it will always be a balance of filling factor, SNR, and available physical space within the magnet bore that must be considered when determining the degree of parallelization via sample capillaries. For comparison, we are sacrificing a factor of ~25 in SNR when using the 15-mm RF coil, compared to a 3-mm coil (since SNR is directly proportional to the filling

factor). However, note that we still save a factor of  $\sim 3$  in measurement time, compared to single sample measurement.

In this work, three regimes were measured in a single measurement: (1) reference experiment of free TFBA in solution in the absence of trypsin, (2) direct binding experiment in the presence of the protein (trypsin), and (3) competitive experiments with the addition BA, whose trypsin binding interaction can be characterized by the displacement of TFBA.<sup>4,17,18</sup> The transverse relaxation time ( $T_2$ ) of  $^{19}\text{F}$  was used to characterize the binding interactions. As a small molecule free in solution, the TFBA  $^{19}\text{F}$   $T_2$  is expected to be relatively long. After binding to a protein, the rotational diffusion will be strongly restricted, which will be reflected in a decrease in the  $T_2$  (equivalently, an increase in  $R_2$ ). As plotted in Figure 7, this was the observed behavior: the TFBA-trypsin complex exhibited slower rotational diffusion than TFBA molecules free in solution ( $R_{2,nc} > R_{2,f}$ ). The TFBA  $R_2$  rates increased 3-fold at the highest trypsin concentration (150  $\mu\text{M}$ ). The addition of BA then displaced TFBA, and  $R_2$  approached the free TFBA value as a greater fraction of TFBA was displaced ( $R_{2,c} \geq R_{2,f}$ ). With a reporter ligand concentration of 25 mM and a target ligand concentration of 1 mM, the contrast was changed by 90%. This suggests that this method is sensitive to target ligand concentrations of  $\ll 1$  mM, to be explored in future work.

Importantly, the  $R_2$  information can be used to extract the dissociation constant of the competitor ligand. This is possible with knowledge of the dissociation constant ( $K_D$ ) of the reporter ligand TFBA (142  $\mu\text{M}$ ), resulting in a calculated  $K_I$  of  $\sim 6$   $\mu\text{M}$  for BA, which indicates that BA is a relatively strong binder to trypsin. Our value is in good agreement with literature values (13–16  $\mu\text{M}$ ) reported under different conditions, using NMR as the analytical method.<sup>17,19</sup>

By parallelization, sample throughput is increased. Using a single MSME experiment, 10–11 echo times could be measured in 58 min (20 scans,  $\text{SNR}_{\text{overall}} = 16$ ), equivalent to an  $R_2$  value measurement time of  $\sim 6$  min per sample (after TR optimization; see the Supporting Information). A typical  $^{19}\text{F}$ -NMR  $T_2$ -relaxation CPMG experiment (10 scans, 11 echo delay times,  $\text{SNR}_{\text{highest}} = 23$ ) required  $\sim 18$  min for one sample with 25 mM TFBA, using standard 5-mm NMR tubes. A factor of 3 is gained in time, without accounting for instrument adjustments, after changing samples nine times. In addition, using capillaries required less material as 150–200  $\mu\text{L}$  of each sample was required, compared to the 500  $\mu\text{L}$  of a typical 5 mm NMR sample tube.

## CONCLUSION AND OUTLOOK

This study presents an MRI-based approach to investigate protein–ligand interactions using a transverse relaxation approach and provides insight relevant to drug discovery applications. A well-soluble fluorinated ligand is required, but neither the protein nor the competitor ligands need to be modified in any way, and the assay is performed in solution.

It shows the opportunity for rapid drug discovery through sample parallelization in space using already available MRI systems. Here, nine samples could be measured in a single experiment, yielding at least a factor of 3 in measurement acceleration compared to standard, single-sample measurements. Measurement times could be further shortened by combining the MRI detection with hyperpolarization of the reporter ligand.<sup>18</sup> Throughput could be increased by several approaches, including rapid  $k$ -space traversal or sparse-sampling techniques,<sup>20–22</sup> increasing sample density within the MR

measurement volume, or by flow-through techniques using sample plugs.<sup>23,24</sup>

## ASSOCIATED CONTENT

### Supporting Information

The Supporting Information is available free of charge at <https://pubs.acs.org/doi/10.1021/acs.analchem.4c00333>.

Additional information on experiment optimization for rapid imaging protocols, and SNR quantification (PDF)

## AUTHOR INFORMATION

### Corresponding Authors

Neil MacKinnon – Institute of Microstructure Technology, Karlsruhe Institute of Technology, D-76344 Eggenstein-Leopoldshafen, Germany; [orcid.org/0000-0002-9362-4845](https://orcid.org/0000-0002-9362-4845); Phone: +49 721 60829307; Email: [neil.mackinnon@kit.edu](mailto:neil.mackinnon@kit.edu); Fax: +49 721 60823928

Jan G. Korvink – Institute of Microstructure Technology, Karlsruhe Institute of Technology, D-76344 Eggenstein-Leopoldshafen, Germany; [orcid.org/0000-0003-4354-7295](https://orcid.org/0000-0003-4354-7295); Phone: +49 721 60829307; Email: [jan.korvink@kit.edu](mailto:jan.korvink@kit.edu); Fax: +49 721 60823928

### Authors

Dilara Faderl – Institute of Microstructure Technology, Karlsruhe Institute of Technology, D-76344 Eggenstein-Leopoldshafen, Germany

Ajmal Chenakkara – Institute of Microstructure Technology, Karlsruhe Institute of Technology, D-76344 Eggenstein-Leopoldshafen, Germany

Mazin Jouda – Institute of Microstructure Technology, Karlsruhe Institute of Technology, D-76344 Eggenstein-Leopoldshafen, Germany; [orcid.org/0000-0002-1226-1174](https://orcid.org/0000-0002-1226-1174)

Alvar D. Gossert – Department of Biology, CH-8093 Zürich, Switzerland

Complete contact information is available at <https://pubs.acs.org/doi/10.1021/acs.analchem.4c00333>

### Notes

The authors declare no competing financial interest.

## ACKNOWLEDGMENTS

J.G.K. and A.D.G. acknowledge support from the ERC-SyG (HiSCORE, 951459). J.G.K., M.J., and N.M. acknowledge support from the DFG-funded CRC 1527 HyPERiON. D.F., A.C., M.J., N.M., and J.G.K. acknowledge partial financial support of the Helmholtz Association through the program Materials Systems Engineering–MSE. D.F. acknowledges additional support of the BioInterfaces International Graduate School (BIF-IGS) at KIT.

## REFERENCES

- (1) Macarron, R.; Banks, M. N.; Bojanic, D.; Burns, D. J.; Cirovic, D. A.; Garyantes, T.; Green, D. V. S.; Hertzberg, R. P.; Janzen, W. P.; Paslay, J. W.; Schopfer, U.; Sittampalam, G. S. *Nat. Rev. Drug Discovery* **2011**, *10*, 188–195.
- (2) Dalvit, C.; Fagerness, P. E.; Hadden, D. T. A.; Sarver, R. W.; Stockman, B. J. *J. Am. Chem. Soc.* **2003**, *125*, 7696–7703.
- (3) Dove, A. W. *Nat. Biotechnol.* **1999**, *17*, 859–863.
- (4) Gossert, A. D.; Jahnke, W. *Prog. Nucl. Magn. Reson. Spectrosc.* **2016**, *97*, 82–125.

- (5) Ross, A.; Schlotterbeck, G.; Senn, H.; von Kienlin, M. *Angew. Chem. (Int. Ed. Engl.)* **2001**, *40*, 3243–3245.
- (6) Hull, W. E.; Sykes, B. D. *J. Mol. Biol.* **1975**, *98*, 121–153.
- (7) Dalvit, C.; Flocco, M.; Veronesi, M.; Stockman, B. J. *Combin. Chem. High Throughput Screen.* **2002**, *5*, 605–611.
- (8) Hennig, J.; Welz, A.; Schultz, G.; Korvink, J.; Liu, Z.; Speck, O.; Zaitsev, M. *Magn. Reson. Mater. Phys., Biol. Med.* **2008**, *21*, 5–14.
- (9) Welz, A.; Coccosco, C.; Dewdney, A.; Gallichan, D.; Jia, F.; Lehr, H.; Liu, Z.; Post, H.; Schmidt, H.; Schultz, G.; et al. *Concepts Magn. Reson. Part B: Magn. Reson. Eng.* **2013**, *43*, 111–125.
- (10) Mispelner, J.; Lupu, M.; Briguët, A. *NMR Probeheads for Biophysical and Biomedical Experiments: Theoretical Principles and Practical Guidelines*; World Scientific Publishing Company, 2015.
- (11) National Electrical Manufacturers Association. *Characterization of Phased Array Coils for Diagnostic Magnetic Resonance Images*. Technical Report, National Electrical Manufacturers Association, 2008; Vol. MS 9–2008 (R2014, R2020); pp 1–16. Available via the Internet at: <https://www.nema.org/Standards/view/Determination-of-Image-Uniformity-in-Diagnostic-Magnetic-Resonance-Images> (accessed on March 18, 2024).
- (12) Lee, Y.; Zeng, H.; Ruedisser, S.; Gossert, A. D.; Hilty, C. J. *Am. Chem. Soc.* **2012**, *134*, 17448–17451.
- (13) Yadav, N. N.; Yang, X.; Li, Y.; Li, W.; Liu, G.; van Zijl, P. C. M. *Sci. Rep.* **2017**, *7*, 10138.
- (14) De Leon-Rodriguez, L. M.; Ortiz, A. V.; Weiner, A. L.; Zhang, S.; Kovács, Z.; Kodadek, T.; Sherry, A. D. *J. Am. Chem. Soc.* **2002**, *124* (14), 3514–5.
- (15) Dalvit, C.; Vulpetti, A. *J. Med. Chem.* **2019**, *62*, 2218–2244.
- (16) Dalvit, C.; Gmür, I.; Rößler, P.; Gossert, A. D. *Prog. Nucl. Magn. Reson. Spectrosc.* **2023**, *138–139*, 52–69.
- (17) Kim, Y.; Hilty, C. *Angew. Chem., Int. Ed.* **2015**, *54*, 4941–4944.
- (18) Kim, Y.; Liu, M.; Hilty, C. J. *Magn. Reson.* **2018**, *295*, 80–86.
- (19) Kasai, K.; Ishii, S. *J. Biochem.* **1978**, *84*, 1061–1069.
- (20) Lazarus, C.; Weiss, P.; Chauffert, N.; Mauconduit, F.; El Gueddari, L.; Destrieux, C.; Zemmoura, I.; Vignaud, A.; Ciuciu, P. *Magn. Reson. Med.* **2019**, *81*, 3643–3661.
- (21) Han, Y.; Sunwoo, L.; Ye, J. C. *IEEE Trans. Med. Imaging* **2020**, *39*, 377–386.
- (22) Yaman, B.; Hosseini, S. A. H.; Moeller, S.; Ellermann, J.; Uğurbil, K.; Akçakaya, M. *Magn. Reson. Med.* **2020**, *84*, 3172–3191.
- (23) Nassar, O.; Jouda, M.; Rapp, M.; Mager, D.; Korvink, J. G.; MacKinnon, N. *Microsyst. Nanoeng.* **2021**, *7*, 30.
- (24) Wouters, B.; Miggiels, P.; Bezemer, R.; van der Crujisen, E. A. W.; van Leeuwen, E.; Gauvin, J.; Houben, K.; Babu Sai Sankar Gupta, K.; Zuijdwijk, P.; Harms, A.; Carvalho de Souza, A.; Hankemeier, T. *Anal. Chem.* **2022**, *94*, 15350–15358.